Entanglement and violation of CHSC Bell's inequality

Edy Alberto Flores Leal, Paul Anton Sigurd Rönnlund, Paula Anna Maria Schembri*

We tested Bell's inequality by generating entangled photon pairs via spontaneous parametric down-conversion (SPDC) using the qutools quED Entanglement Demonstrator. We characterized the source with nonentangled photon pairs, measuring visibilities in the horizontal and diagonal bases. We repeated the measurements for entangled photon pairs in the $|\Phi^-\rangle$ and $|\Phi^+\rangle$ states. Setting sixteen polarization combinations, we obtained a correlation parameter of $|S| = 2.59 \pm 0.04$, confirming the violation of Bell's inequality.

* *All the authors contributed equally.*

1. Introduction

Quantum entanglement is a fundamental feature of quantum mechanics, characterized by non-classical correlations between the states of two or more particles. When two particles are entangled, the measurement of one immediately affects the state of the other, regardless of the distance between them. This nonlocal behavior, which Einstein famously criticized as "spooky action at a distance," seemed to allow information to travel faster than light. This apparent violation of locality led Einstein, Podolsky, and Rosen to question the completeness of quantum mechanics in 1935, proposing that hidden variables might underlie the observed correlations [1].

In 1964, John Bell demonstrated that entanglement was an inherently nonlocal phenomenon [2]. His work led to the formulation of Bell's inequality, a crucial test for the incompatibility of quantum mechanics and local hidden-variable theories. Several versions of the inequality exist, but one of the most widely used to test this theorem is the Clauser–Horne–Shimony–Holt (CHSH) inequality [3]:

$$|S(\alpha,\alpha',\beta,\beta')| = |E(\alpha,\beta) + E(\alpha',\beta) + E(\alpha,\beta') + E(\alpha',\beta')| \leq 2. \tag{1}$$

Here, α, α' and β, β' denote the polarizing filter orientation placed along the two arms of the source, while $E(\alpha,\beta)$ is the quantum correlation, defined as the expectation value of the product of the experimental "outcomes." The correlation function is determined from the coincidence counts $C(\alpha,\beta)$ as

$$E(\alpha,\beta) = \frac{C(\alpha,\beta) - C(\alpha,\beta_\perp) + C(\alpha_\perp,\beta) + C(\alpha_\perp,\beta_\perp)}{C(\alpha,\beta) + C(\alpha,\beta_\perp) + C(\alpha_\perp,\beta) + C(\alpha_\perp,\beta_\perp)}, \tag{2}$$

where $\alpha_\perp$ and $\beta_\perp$ denote polarizer settings orthogonal to α and β, respectively. In this experiment, we investigated the violation of the CHSH inequality using polarization-entangled photon pairs generated by the qutools quED Entanglement Demonstrator. We measured the correlation functions for various polarizer settings and computed the CHSH parameter S.

2. Experiment

2.1. Experimental setup

The experimental setup used to produce entangled photon pairs is shown in Fig. 1. In this setup, a blue, high-energy pump laser emits photons that split into a pair of red, low-energy photons. The splitting occurs because of the interaction with a type-I β-barium borate (β-BBO) nonlinear crystals due to energy and momentum conservation [4]. This conversion happens with a low frequency (of the order of 10^{-11}). For this setup, two crystals are positioned with their optical axes oriented orthogonally, and the interaction leads to a process called spontaneous parametric down-conversion (SPDC). To initiate SPDC, the setup has a half-wave plate placed before the crystals to linearly polarize the pump beam at 45°. This polarization ensures a 50% chance that the pump photon undergoes down-conversion in either crystal, producing the entangled state

$$|\Phi\rangle = \frac{1}{\sqrt{2}}(|\mathrm{H}\rangle_1|\mathrm{H}\rangle_2 + \mathrm{e}^{\mathrm{i}\phi}|\mathrm{V}\rangle_1|\mathrm{V}\rangle_2), \tag{3}$$

where $|\mathrm{H}\rangle$ and $|\mathrm{V}\rangle$ denote horizontal and vertical polarization states, respectively; ϕ is the relative phase dependent on the phase matching and thickness of the crystal [4].

From Fig. 1, the two BBO crystals are at different distances. Also, BBO crystals are birefringent. Both features cause the photon pairs to experience decoherence and temporal delays because of group-velocity mismatch and dispersion effects. The setup preserves coherence and ensures high entanglement fidelity by placing birefringent YVO_4 crystals; one precompensates the temporal walk-off between polarization components before SPDC, and the other one postcompensates to equalize the path length difference accumulated in the two orthogonal BBO crystals.

Subsequently, the entangled photon pair exits the crystal setup. Each photon travels through separate optical arms, where mirrors and adjustable polarizers direct each photon in the system. To detect these photons, the system employs silicon avalanche photodiodes coupled via long-pass filters and single-mode fibers. The first one blocks residual laser-diode light, while the second erases all spatial information related to the distinguishability of the information. Finally, the computer records single-photon events at each arm, as well as the coincidences between the two.

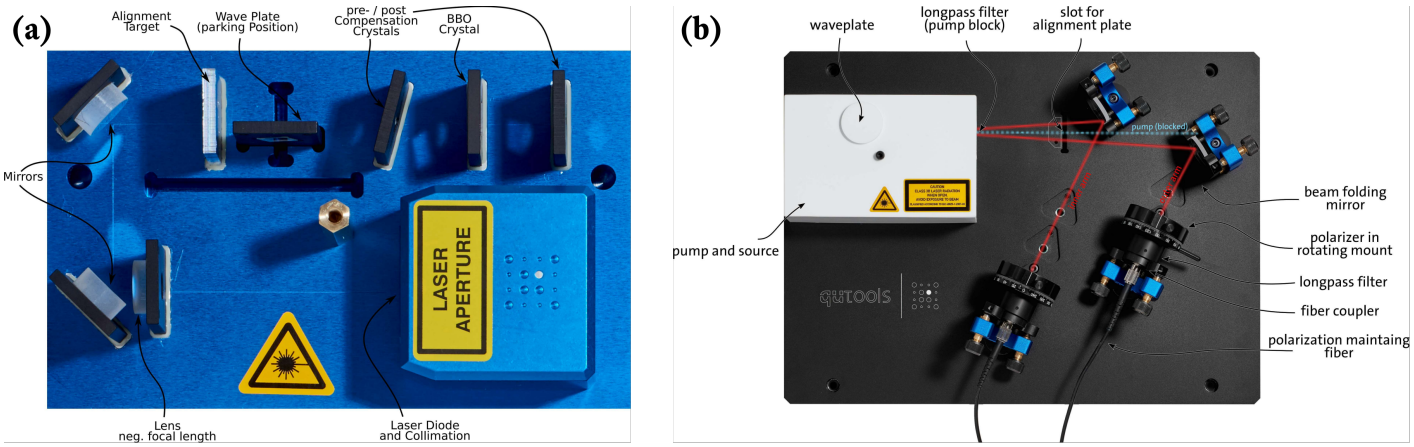

Figure 1: (a) Crystal configuration of the setup. The laser is directed into a crystal array where the pre- and post-compensating crystals compensate for coherence losses in the BBO. The BBO will, through spontaneous parametric down-conversion, generate entangled photon pairs. **(b) Processing of the two entangled photon beams**. Mirrors direct the beams into adjustable polarizers, and then into detectors with long-pass filters and single-mode fibers to maintain polarization. The beams are directed into a "stopwatch" for processing.

2.2. Experimental methods

We began the experiment by the source characterization using non-entangled photon pairs. We measured the coincidence counts and visibility in both HV and DA bases. We estimated the visibility using the following expression:

$$V = \frac{C_{\parallel} - C_{\perp}}{C_{\parallel} + C_{\perp}}. \tag{4}$$

Here, $C_{\parallel}$ and $C_{\perp}$ represented the extrema of the coincidence count rates. To estimate the error ΔV, we used the Gaussian error propagation rule given by

$$\Delta V = \left[\left(\frac{\partial V}{\partial C_{\parallel}} \Delta C_{\parallel} \right)^2 + \left(\frac{\partial V}{\partial C_{\perp}} \Delta C_{\perp} \right)^2 \right]^{\frac{1}{2}}, \tag{5}$$

where $\Delta C_{\parallel} = \sqrt{C_{\parallel}}$ and $\Delta C_{\perp} = \sqrt{C_{\perp}}$, and

$$\frac{\partial V}{\partial C_{\parallel}} = \frac{2C_{\perp}}{(C_{\parallel} + C_{\perp})^2}, \tag{6}$$

$$\frac{\partial V}{\partial C_{\perp}} = -\frac{2C_{\parallel}}{(C_{\parallel} + C_{\perp})^2}, \tag{7}$$

Using these parameters, we determined the experimental visibility, $V^{\text{exp}}_{\text{basis}} = V \pm \Delta V$.

To approximate the efficiency of the detectors of each arm, we used the fact that the count rate is proportional to the pump intensity and the detector efficiency. The coincidence rate is then proportional to pump intensity, as well as the efficiency of each detector,

$$\text{CR}_i \propto I\eta_i, \tag{8}$$

$$C_{12} \propto I\eta_1\eta_2, \tag{9}$$

and to determine the efficiencies, we take into account the dark counts:

$$\eta_1 \approx \frac{C_{12}}{\text{CR}_2 - D_2}, \tag{10}$$

$$\eta_2 \approx \frac{C_{12}}{\text{CR}_1 - D_1}. \tag{11}$$

Here, CR_i denotes the count rate at each arm, and C_{12} is the coincidence rate at both detectors. D_1 and D_2 represent the dark counts at each arm. This approximation takes all different losses into account (fiber losses, coupling losses, and others) since it is based on the actual performance of the detector. Every loss affects the count and coincidence rates, which will affect the efficiency approximation. To estimate the error, we once again use the Gaussian error propagation rule:

$$\Delta\eta_1 = \left[\left(\frac{\partial \eta_1}{\partial C_{12}} \Delta C_{12} \right)^2 + \left(\frac{\partial \eta_1}{\partial \text{CR}_2} \Delta \text{CR}_2 \right)^2 + \left(\frac{\partial \eta_1}{\partial D_2} \Delta D_2 \right)^2 \right]^{\frac{1}{2}} \tag{12}$$

where $\Delta C_{12} = \sqrt{C_{12}}$, $\Delta \text{CR}_2 = \sqrt{\text{CR}_2}$, $\Delta D_2 = \sqrt{D_2}$, and

$$\frac{\partial \eta_1}{\partial \text{CR}_2} = -\frac{C_{12}}{(\text{CR}_2 - D_2)^2}, \tag{13}$$

$$\frac{\partial \eta_1}{\partial C_{12}} = \frac{1}{\text{CR}_2 - D_2}, \tag{14}$$

$$\frac{\partial \eta_1}{\partial D_2} = \frac{C_{12}}{(\text{CR}_2 - D_2)^2}. \tag{15}$$

To get the error of η_2, we switch all 1's above to 2's, and vice versa.

The next step was fixing a polarizer at the H state while the other was rotated in 5° steps to examine the behavior of the coincidence

counts against the polarization. After characterizing the source, we generated entangled photon pairs and prepared the Bell states $|\Phi^-\rangle$ and $|\Phi^+\rangle$. This was achieved by inserting a HWP in front of the pump and then rotating it, respectively. Next, we repeated the previous coincidence count and visibility measurements. We recorded coincidence counts for sixteen polarization combinations (shown in table 1) and experimentally evaluated the S parameter to test Bell's inequality.

Table 1: Different polarization combinations to measure the CHSH inequality

α	β	α	β
0°	22.5°	45°	22.5°
0°	67.5°	45°	67.5°
0°	112.5°	45°	112.5°
0°	157.5°	45°	157.5°
90°	22.5°	135°	22.5°
90°	67.5°	135°	67.5°
90°	112.5°	135°	112.5°
90°	157.5°	135°	157.5°

We used Eq. (1) to compute the S parameter, and its statistical error was computed using Gaussian error propagation:

$$\Delta E = \frac{2[C(\alpha,\beta)+C(\alpha_\perp,\beta_\perp)][C(\alpha,\beta_\perp)+C(\alpha_\perp,\beta)]}{[C(\alpha,\beta)+C(\alpha,\beta_\perp)+C(\alpha_\perp,\beta)+C(\alpha_\perp,\beta_\perp)]^2} \times \sqrt{\frac{1}{C(\alpha,\beta)+C(\alpha_\perp,\beta_\perp)}+\frac{1}{C(\alpha,\beta_\perp)+C(\alpha_\perp,\beta)}}. \tag{16}$$

Both expressions were automatically computed by the quED system once we set the sixteen polarization combinations.

3. Results and discussion

We began the experiment by characterizing the source. We recorded the following dark counts in both detectors:

$$D_1 = 3250, \tag{17}$$
$$D_2 = 2970. \tag{18}$$

The maximized count and coincidence rates were measured when the polarizers were both set to 90°, and are displayed below:

Table 2: Measurements made with polarizers at 90°

Chanel 1	Chanel 2	Coincidence rate
97202	115150	3271

To minimize errors in the efficiency approximation, we used a value as large as possible. Plugging these values into the above formulas, we got:

$$\eta_1 = 2.9 \pm 0.5\% \tag{19}$$
$$\eta_2 = 3.5 \pm 0.6\% \tag{20}$$

These detector efficiencies are a source of error moving forwards, a count statistics one. The efficiencies are significantly low, and high losses can be expected in the rest of the experiment.

In order to determine the input laser's polarization, we measured coincidence counts without a HWP in the HV basis and the AD basis shown in Table 3.

Table 3: Coincidence counts for each basis

Setting	C_{HH}	C_{HV}	C_{VH}	C_{VV}
Coin. counts	3271	31	20	5

Setting	C_{DD}	C_{DA}	C_{AD}	C_{AA}
Coin. counts	850	504	710	480

From the table, we concluded that the polarization after the BBO crystal is horizontal $|\mathrm{H}\rangle$, which means that the input laser's polarization is vertical $|\mathrm{V}\rangle$ due to the crystal being type-I. Then, we calculated the parallel and perpendicular coincidence counts as shown in Table 4:

Table 4: Coincidence counts for each α and β polarization combinations in the HV and DA bases without HWP

Coin. counts	**HV basis**	**DA basis**
$C_\parallel$	3276	1330
$C_\perp$	51	1214

For the HV basis, we used the quantities

$$C_\parallel = C_{\mathrm{HH}} + C_{\mathrm{VV}}, \tag{21}$$
$$C_\perp = C_{\mathrm{HV}} + C_{\mathrm{VH}} \tag{22}$$

where $\mathrm{H} \equiv 90^\circ$ and $\mathrm{V} \equiv 0^\circ$ for the polarization settings $\alpha, \beta \in \{0^\circ, 90^\circ\}$, and the quantities

$$C_\parallel = C_{\mathrm{DD}} + C_{\mathrm{AA}}, \tag{23}$$
$$C_\perp = C_{\mathrm{DA}} + C_{\mathrm{AD}} \tag{24}$$

for the DA basis, where $\mathrm{D} \equiv 45^\circ$ and $\mathrm{A} \equiv -45^\circ$ for the different polarization configurations $\alpha, \beta \in \{-45^\circ, 45^\circ\}$. Here, α denoted the polarization in the left arm, and β for the polarization in right arm. Therefore, the experimental visibilities on the HV and DA bases without HWP were

$$V_{\mathrm{HV}}^{\mathrm{exp}} = 96.93 \pm 0.43\%, \tag{25}$$
$$V_{\mathrm{DA}}^{\mathrm{exp}} = 4.56 \pm 1.98\%. \tag{26}$$

The next step was fixing one polarizer to be in the H state and then rotating the second polarizer by steps of 5°. We shown the observed behavior of the coincidence counts against the polarization in Fig. 2 (a).

As known from the theory [4], the probability that one particle passes a polarizer under the angle α and a second particle passes

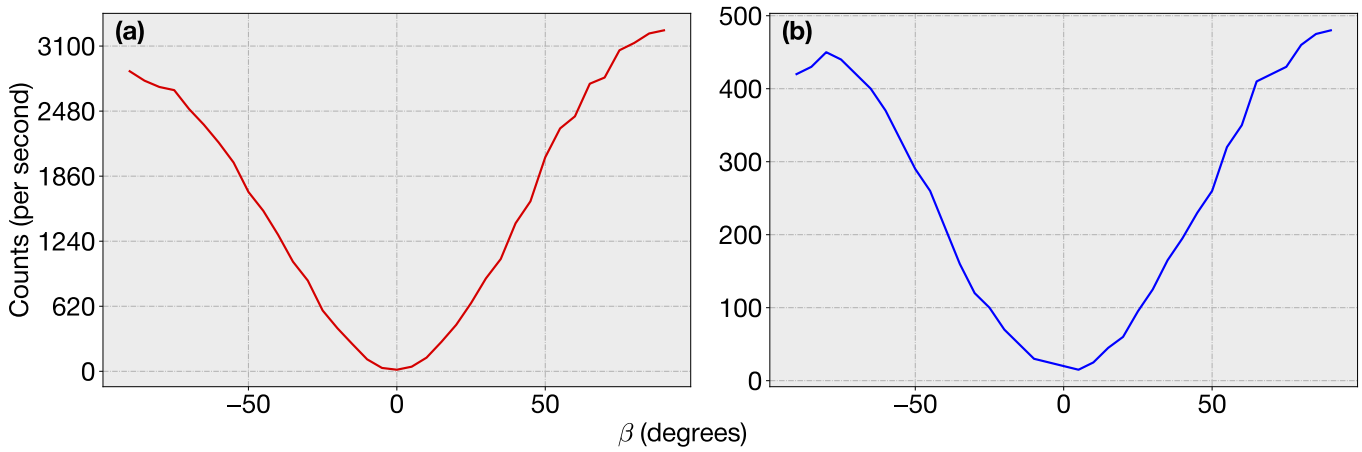

Figure 2: Coincidence counts against polarization for a fixed polarizer in the H state. **(a)** shows the behavior when no HWP was used, and **(b)** shows the case when a HWP was inserted. Both curves show the expected $\cos^2(\theta)$ nature from the theory, but the second curve has a significant decrease in the counts per second measured.

a polarizer under the angle β is given by

$$P(\alpha, \beta) = \frac{1}{2}\cos^2(\alpha - \beta). \tag{27}$$

It is relevant to mention that we usually measure the coincidence rate instead of probabilities, as it has been done in this report. We noticed that the maximum coincidence count was achieved when $\alpha \approx \beta$, as expected from Eq. (27). However, we do not have a completely symmetric plot, likely be due to error in the angular setting of the polarizers. Once the source has been characterized, we proceeded to create the Bell states. We inserted the HWP in front of the pump and measured the coincidence rates in the HV and DA bases, as shown in Table 5:

Table 5: Coincidence counts for each α and β polarization combinations in the HV and DA bases with HWP

Coin. counts	HV basis	DA basis
$C_{\parallel}$	605	87
$C_{\perp}$	36	410

Thus, the visibilities obtained in both bases when using a HWP were the following:

$$V_{\mathrm{HV}}^{\mathrm{exp}} = 88.77 \pm 1.82\%, \tag{28}$$
$$V_{\mathrm{DA}}^{\mathrm{exp}} = 64.99 \pm 3.41\%. \tag{29}$$

Once again, we fixed one polarizer to be in the H state and rotated the second polarizer in steps of 5°, shown in Fig. 2 (b). This time, we noticed that the measured visibility in the HV basis slightly decreased while the visibility in the DA basis increased significantly.

We recall that the Bell states $|\Phi^{\pm}\rangle$ are

$$\begin{aligned} |\Phi^+\rangle &= \frac{1}{\sqrt{2}}(|\mathrm{H}\rangle_1 |\mathrm{H}\rangle_2 + |\mathrm{V}\rangle_1 |\mathrm{V}\rangle_2) \\ &= \frac{1}{\sqrt{2}}(|\mathrm{D}\rangle_1 |\mathrm{D}\rangle_2 + |\mathrm{A}\rangle_1 |\mathrm{A}\rangle_2), \\ |\Phi^-\rangle &= \frac{1}{\sqrt{2}}(|\mathrm{H}\rangle_1 |\mathrm{H}\rangle_2 - |\mathrm{V}\rangle_1 |\mathrm{V}\rangle_2) \\ &= \frac{1}{\sqrt{2}}(|\mathrm{D}\rangle_1 |\mathrm{A}\rangle_2 + |\mathrm{A}\rangle_1 |\mathrm{D}\rangle_2). \end{aligned} \tag{30}$$

For this measurement, we noticed that the parallel counts in the HV basis and the orthogonal counts in the DA basis are the highest. Therefore, we identified the generation of the $|\Phi^-\rangle$ state. Another significant difference to the state without the HWP, is that the maximum coincidence rate is significantly lower, ~ 500 compared to ~ 3000 before. This is most likely due to less SPDC happening in either of the two BBO crystals.

Before the HWP was inserted, the incoming light was either down converted in one BBO crystal or the other, modified by their efficiencies. After the polarization was turned in the HWP, the incoming light has equal chance of being down converted in either the first or the second BBO, making the overall conversion rate lower, and thus decreasing the coincidence counts. The HWP does ensure a higher visibility, with the drawback of lower coincidence rates [4, 5].

The next task consisted on rotating the HWP by 180° and repeating the previous measurements, obtaining the following results:

Table 6: Coincidence counts for each α and β polarization combinations in the HV and DA bases with HWP, rotated 180°

Coin. counts	HV basis	DA basis
$C_{\parallel}$	1660	1130
$C_{\perp}$	70	195

The measured visibilities gotten for HV and DA bases using a rotated HWP were

$$V_{\mathrm{HV}}^{\mathrm{exp}} = 91.91 \pm 0.95\%, \tag{31}$$
$$V_{\mathrm{DA}}^{\mathrm{exp}} = 70.57 \pm 1.95\%. \tag{32}$$

Compared to the initial HWP alignment, we obtained higher coincidence counts in the parallel setting for both HV and BA bases. This implied the generation of the $|\Phi^+\rangle$ state. Finally, we recorded the coincidences for sixteen different polarizer combinations presented in Table 1. By doing so, we tested Bell's inequality and got the $|S|$ parameter

$$|S| = 2.59 \pm 0.04 \tag{33}$$

for an integration time of $\Delta t = 1000$ ms. Since the statistical error falls in the range of the inequality $S > 2$, we confirmed the violation of the Bell inequality.

It is relevant to mention that there are several (possible) sources of errors that lead to the unsatisfactory experimental results. For instance, the wrong manipulation of the experimental apparatuses, i.e., polarization misalignments, could be one of the main error sources. Also, there are a couple environmental factors like background noise coming from other light sources. Finally, something that was not taken into account was the accidental coincidence rate. These factors could hinder the quality of the experimental measurements and further research is needed to identify their impact in the experimental outcomes.

4. Conclusions

To summarize, we determined the input laser's polarization to be vertical, generated the $|\Phi^{\pm}\rangle$ states, and demonstrated the incompatibility of quantum mechanics and local hidden-variable theories by the CHSH inequality violation by several standard deviations. On the other hand, making multiple measurements per data point, taking the average, and obtaining error bars for each figure are some areas of improvement.

References

[1] Einstein, A., Podolsky, B. & Rosen, N. Can Quantum-Mechanical Description of Physical Reality Be Considered Complete? *Physical Review* **47**, 777–780 (1935). URL http://dx.doi.org/10.1103/PhysRev.47.777.

[2] Bell, J. S. On the Einstein Podolsky Rosen paradox. *Physics Physique Fizika* **1**, 195–200 (1964). URL https://link.aps.org/doi/10.1103/PhysicsPhysiqueFizika.1.195.

[3] Clauser, J. F. & Horne, M. A. Experimental consequences of objective local theories. *Physical Review D* **10**, 526–535 (1974). URL http://dx.doi.org/10.1103/PhysRevD.10.526.

[4] QuTools. quED manual (2021). URL https://www.qutools.com/files/quED/quED_manual.pdf.

[5] Hodelin, J. F., Khoury, G. & Bouwmeester, D. Optimal generation of pulsed entangled photon pairs. *Physical Review A* **74** (2006). URL http://dx.doi.org/10.1103/PhysRevA.74.013802.